

Localized Energy States Induced by Atomic-Level Interfacial Broadening in Heterostructures

Anis Attiaoui,^{1,*} Gabriel Fettu,^{1,*} Samik Mukherjee,¹ Matthias Bauer,² and Oussama Moutanabbir^{1,†}

¹*Department of Engineering Physics, École Polytechnique de Montréal,
C.P. 6079, Succ. Centre-Ville, Montréal, Québec, Canada H3C 3A7*

²*Applied Materials Inc., 974 E. Arques Avenue, Sunnyvale, CA 94085, USA*

A theoretical framework incorporating atomic-level interfacial details is derived to include the electronic structure of buried interfaces and describe the behavior of charge carriers in heterostructures in the presence of finite interfacial broadening. Applying this model to ultrathin heteroepitaxial $(\text{Si}_{1-x}\text{Ge}_x)_m/(\text{Si})_m$ superlattices predicts the existence of localized energy levels in the band structure induced by sub-nanometer broadening, which provides additional paths for hole-electron recombination. These predicted interfacial electronic transitions and the associated absorptive effects are confirmed experimentally at variable superlattice thickness and periodicity. By mapping the energy of the critical points, the optical transitions are identified between 2 and 2.5 eV thus extending the optical absorption to lower energies. This phenomenon enables a straightforward and non-destructive probe of the atomic-level broadening in heterostructures.

Interfaces are ubiquitous in design and processing of a variety of low-dimensional systems and devices [1–3]. Their characteristic features such as strain field, composition, and topology are known to depart from the idealized picture of atomically flat and abrupt joint surfaces [3–6]. The nature of these smeared interfaces impacts the behavior of charge carriers and shape the overall optical and electronic characteristics. These effects become even more prominent as the device dimension shrinks and the operating principles involve subtle quantum processes. For instance, the three-dimensional interfacial roughness has been shown to influence the confinement of charge carriers and their wavelength spread across one or more interfaces. As a matter of fact, this roughness must be considered to accurately describe the scattering mechanisms and predict the heterostructure optoelectronic properties [3, 7, 8]. This interplay between interfacial roughness and carrier scattering has also been critical in the design of highly scaled nanosheet transistors and spin qubits [9, 10]. In the latter, for instance, the atomic-level disorder at a quantum well interface was found to induce a large spread in valley splitting energy thereby hindering the uniformity of electron spin qubits [10].

It is clear that the behavior of charge carriers in heterostructures is shaped by the interfacial broadening, which is typically on the order of a few monolayers (ML) [4–6]. Herein, we argue that this atomic-level broadening creates localized energy levels yielding a distinct optical transition. Using SiGe/Si as a model system, Figure 1(a) illustrates the basic band-to-band absorption for a type-I SiGe/Si quantum well (QW) along with the localized energy levels induced in the band structure at the interface. These levels provide additional paths for electron-hole recombinations, as highlighted by the direct transition, labeled hereafter $E_{4\tau}$ (Fig. 1(a), inset). In principle, this transition would manifest as an additional absorption signature at lower energy when compared to the main interband critical point (CP) absorption peak (E_{CP}).

To evaluate the hypothesized interface-related changes in the band structure, a framework was first implemented to quantitatively include the absorptive effects of buried interfaces. The miniband structure as well as the electron and hole wavefunctions are calculated within the 14-band $k \cdot p$ formalism, where the microscopic effect of the interface is accounted for through the interface asymmetry Hamiltonian (H_{IF}) [11–13]. Both Si-on-SiGe and SiGe-on-Si interfaces are considered in H_{IF} . Since in Si-rich SLs the lowest conduction band (CB) has the $\Gamma_4^-/(\Gamma_8^- + \Gamma_6^-)$ symmetry and the Γ_2^- CB is close in energy, the four lowest CBs were considered for an accurate simulation of the interband absorption [14]. To that end, a new CB parametrization for Si and $\text{Si}_{1-x}\text{Ge}_x$ alloys was developed within the 14-band $k \cdot p$ theory; see [Supplemental Material](#) [15]. The optical transition energies are calculated between electron and hole minibands based on crystal momentum conservation, and the electron-hole wavefunction overlap integral indicates which transitions are strongly active in absorption. The interface width (4τ) was varied between 0 and a few ML to capture the broadening effects, where $4\tau = 0$ corresponds to an abrupt interface.

Figure 1(b) displays the calculated absorption coefficient (α in cm^{-1}) for a $\text{Si}_{0.71}\text{Ge}_{0.29}/\text{Si}$ QW at different values of 4τ between 0 and 0.32 nm. The well thickness (t_w) was fixed at 2 nm. Interestingly, non-zero interfacial widths were found to yield a distinct absorption peak below 3 eV whose energy redshifts as 4τ increases. This behavior is confirmed by evaluating the interface contribution to α for two sets of $(\text{Si}_{0.73}\text{Ge}_{0.27})_m/(\text{Si})_m$ SLs with a periodicity $m = 3$ and 16 and a fixed total thickness of 60 nm. These SLs are labeled hereafter as S_m . The well thickness in S_3 and S_{16} is 7 nm and 2 nm, respectively. The obtained polarized-dependent absorption coefficients are displayed in Fig. 1(c, d), where $\alpha_{\text{Total-IF}}$ is defined as $2\alpha_{\text{TE}} + \alpha_{\text{TM}}$. Note that the stronger the interface potential, the greater is the interface state energy. Furthermore, the intensity of the interface-related transitions is higher

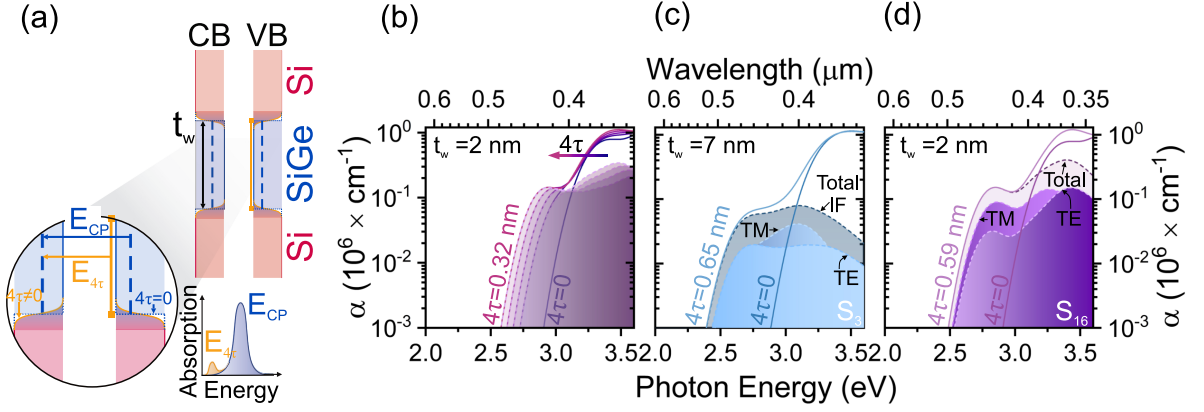


FIG. 1. **The predicted effect of interfacial broadening on the optical absorption.** (a) Schematic representation of a SiGe/Si QW with (orange) and without (blue) the effect of interfaces broadening. The QW has a thickness of t_w . The zoom-in inset highlights both possible optical transitions. (b) Next, the 14-band $k \cdot p$ absorption coefficient (α) of the QW with a variable interfacial broadening 4τ from 0 to 0.32 nm with a 0.1 nm step. TE and TM polarization-dependent absorption coefficient (α) of 2 SLs: (c) S_3 and (d) S_{16} with APT-measured input parameters (thicknesses: $S_3 \rightarrow t_w = 7.3 \pm 0.2 \text{ nm}$, $S_{16} \rightarrow t_w = 2.2 \pm 0.3 \text{ nm}$, interfacial width (4τ): $S_3 \rightarrow 0.65 \pm 0.10 \text{ nm}$, $S_{16} \rightarrow 0.59 \pm 0.20 \text{ nm}$, Ge content: $S_3 \rightarrow 29.3 \pm 2.3 \%$, $S_{16} \rightarrow 24.7 \pm 3.0\%$).

in S_{16} superlattice (SL) than S_3 , which reflects the relative importance of the interface as t_w of S_{16} ($\sim 2 \text{ nm}$) is thinner than that of S_3 ($\sim 7 \text{ nm}$). Additionally, α_{TM} is broader in S_3 than S_{16} . This is directly associated to the number of available interface-related transitions. In fact, there are fewer confined CB states in S_{16} than in S_3 , which are converted to interface-promoted transitions, hence the sharper absorption coefficient. Therefore, the effect of interfaces is more prominent for thinner layers.

To evaluate experimentally the theoretical findings, a series of ultra-short SiGe/Si SLs were epitaxially grown at a Ge content below 30% in a reduced-pressure chemical vapor deposition (RPCVD) reactor. Four $(\text{Si}_{1-x}\text{Ge}_x)_m/(\text{Si})_m$ SLs with different periodicity $m = 3, 6, 12$, or 16 were investigated. S_{16} and S_{12} were grown at 650°C , S_6 at 600°C , and S_3 at 500°C [44]. Figure 2(a) shows the high-angle annular dark field scanning transmission electron microscopy (HAADF-STEM) image of S_3 along with Ge concentration profile obtained using atom probe tomography (APT). A representative 3D atom-by-atom APT reconstruction map is also displayed in Fig. 2(b). APT analysis was exploited to quantify the interfacial width 4τ and the atomic content in each layer of the SLs by following the procedure described in Ref.[48]. The SiGe/Si stack is fully strained with an average degree of strain relaxation of 5.4%. Additionally, surface roughness (RMS) was measured by atomic force microscopy (AFM). Details of structural characterization are shown in Supplemental Material [15]. The interband optical absorption of the SLs was measured at room temperature by variable angle spectroscopic ellipsometry (SE). The ellipsometric parameters Ψ and Δ are acquired at an angle of incidence (AOI) between 55° and 80° with a 5° step covering photon energy ω from 1.5 to 6 eV. Since the SL region has distinct

optical properties than its constituent materials, the SL is modeled as a single layer with its own unique set of optical constants [49–51].

The “wavelength-by-wavelength” energy-dependent complex dielectric functions ($\tilde{\epsilon} = \epsilon_1 + i\epsilon_2$) are shown for all SLs in Fig. 2; more details in Supplemental Material [15]. Moreover, overlaid in Fig. 2(c,d) are the data for bulk Ge [45] (dashed-black), bulk Si [46] (gray-dotted line) and fully strained, 90 nm thick $\text{Si}_{0.73}\text{Ge}_{0.27}$ [47] dielectric functions (gray dash-dotted). The intensity range of the optical properties of all SLs as well as the main spectral CP (E_2, E'_0) positions qualitatively agree with those of bulk materials. The SL-embedded $\text{Si}_{1-x}\text{Ge}_x$ layers play an important role in modulating $\tilde{\epsilon}$ of the whole SL given that its intensity is between that of bulk Si and bulk Ge. Furthermore, the E_1 band edge for the $\text{Si}_{0.73}\text{Ge}_{0.27}$ dielectric function has an onset of 2.92 eV to reach an inflection point near 3.2 eV. For a Ge content below 30%, the E_1 CP is a superposition between the Si E'_0 CP located at 3.35 eV [43] and the SiGe E_1 CP.

The dielectric functions of all SLs clearly indicate the presence of an additional broad low-intensity peak below 3 eV that is absent in both Si bulk and SiGe thin film. Only Ge bulk exhibits a strong CP near 2.1 eV related to the E_1 transition occurring along the eight equivalent [111] directions of the Brillouin zone (dashed-black line in Fig. 2(c)). The observed SL-related CP peak position between 2 and 2.5 eV agrees well with the theoretical predictions highlighted in Fig. 1(b-d). Thus, the origin of this CP, henceforth labeled as $E_{4\tau}$, will be discussed in light of the interfacial broadening. The blue and green insets in Fig. 2(c, d) are zoom-in log-log plots, between 1.5 eV and 3 eV, confirming the overlap between the CP energy and the calculated $E_{4\tau}$ transition. The $E_{4\tau}$, E'_0 and E_1 CPs

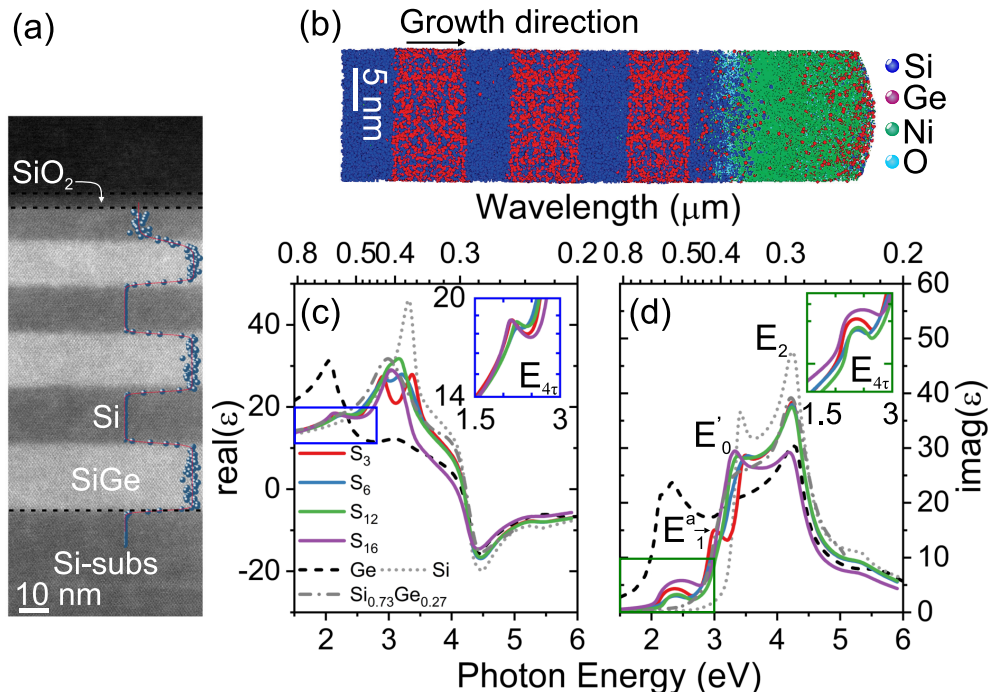


FIG. 2. **Structural and optical characterization.** HAADF-STEM image of the $(\text{Si}_{0.71}\text{Ge}_{0.29})_3/(\text{Si})_3$ SL overlaid with the concentration profile of Ge extracted from the corresponding APT 3D reconstruction shown in panel (b). The average well and barrier thicknesses were estimated by APT to be 7.3 ± 0.2 nm and 6.0 ± 0.2 nm, respectively. (c) The real (ϵ_1) and imaginary (ϵ_2) part of the complex dielectric function of the four $(\text{Si}_{1-x}\text{Ge}_x)_m/(\text{Si})_m$ SLs with increasing periodicity $m(= 3, 6, 12, 16)$ are presented. The Ge [45], Si [46] bulk and 90 nm thick $\text{Si}_{0.73}\text{Ge}_{0.27}$ [47] dielectric functions are also shown for comparison purposes. The blue and green insets are log-log plot of ϵ_1 and ϵ_2 , respectively between the energy range (1.5 – 3 eV). They highlight the interfacial broadening related optical transition $E_{4\tau}$.

in Fig. 2(c, d) are analyzed in Fig. 3. The second order dielectric function derivatives as well as the corresponding fits for the CPs are also shown for all the SLs. The generic standard critical-point lineshape model [43, 52] was used to fit the second derivative of $\tilde{\epsilon}$. The real and imaginary parts of $(d^2\tilde{\epsilon}/d\omega^2)$ were fitted simultaneously using a global optimization procedure based on the differential evolution (DE) algorithm, as specified in Supplemental Material [15]. Additionally, the obtained CP energies are shown for each SL as a vertical red line.

The $E_{4\tau}$ transition is a distinct peak in $d^2\tilde{\epsilon}/d\omega^2$ between 2 eV and 2.5 eV for all the $(\text{Si}_{1-x}\text{Ge}_x)_m/(\text{Si})_m$ SLs. Mass periodicity in the growth direction of SLs has long been recognized at the origin of phenomena such as zone folding and quantum confinement [53]. Therefore, in order to eliminate SL symmetry as an origin of the $E_{4\tau}$, it is crucial to address any other plausible mechanisms. Firstly, quantum confinement should be excluded. Indeed, as SiGe thickness increases (m decreases), the $E_{4\tau}$ transition energy decreases at a rate smaller than a confinement-related effect. For instance, consider the following hypothetical SL, with $m= 3$, similar to S_3 , with a fixed Si barrier thickness of 6 nm and a variable t_w (between 5 and 9 nm). While suppressing any interfacial broadening,

the absorption band edge redshifts within an energy range of 10 meV as t_w increases; see Supplemental Material [15]. The absence of any intrinsic additional peak below 3 eV proves that quantum confinement cannot be responsible of the observed $E_{4\tau}$ transition. Secondly, the observed CP transition located between 2 eV and 2.5 eV can neither be explained by any of the E_1 CP of the individual layers (Si or SiGe, be it relaxed or strained) nor by a superposition of the $E_1 + \Delta_1$ transition of SiGe and the E_1 transition in Si. The E_1 transition in $\text{Si}_{1-x}\text{Ge}_x$ was found to be located between 3.075 and 2.850 eV for a Ge content between 20% and 30% which is still higher in energy than the observed $E_{4\tau}$ transition [54]. Besides, the $E_1 + \Delta_1$ transition in SiGe alloys is only resolved for a Ge content above 32%, which eliminates any possibility for the $E_1 + \Delta_1$ transition to originate from within the SiGe sublayer, as all SLs have an average Ge content below 30% [47, 55–57]. Thirdly, if the E_1 and $E_1 + \Delta_1$ transition in Ge are considered, then a superposition with E_1 transition from Si or SiGe can lead to a reasonable explanation of the $E_{4\tau}$ transition. However, this hypothesis is unlikely due to the absence of any Ge segregation near the interfaces as confirmed by APT. Moreover, similar to early studies on Si [43], a 2D CP was used for all CPs except the $E_{4\tau}$ transition, for

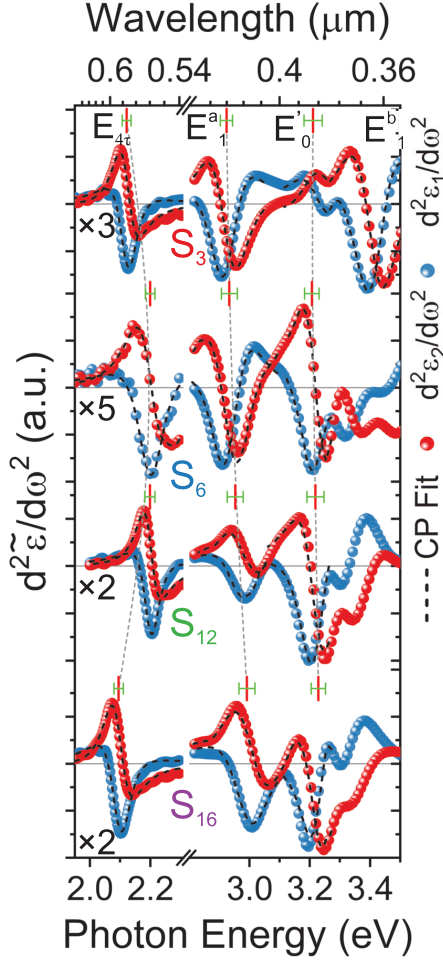


FIG. 3. **Second derivative CP analysis.** The second derivative of $\tilde{\epsilon}$ as well as the CP lineshape fit (dashed-black lines). The energy error bars are a combination between the SE experimental error (~ 5 meV) and the 95% confidence fit error. The dashed-gray lines are a guide to the eye for the evolution of the CPs as a function of the SL periodicity m . The vertical red lines are the peak position for each CP, evaluated from the fit. Note that the vertical scale has to be divided by the factor given under each spectrum.

which a 3D CP was used. This observation is confirmed throughout the analysis of all SLs, where a 3D transition gave a good quality fit with R^2 higher than 0.985. The dashed-gray lines in Fig. 3 show the shift in the critical energy peak position as the SL periodicity changes. Increasing the periodicity up to 12 periods leads to a small blueshift of 7.6 meV $E_{4\tau}$, followed by a redshift at the highest periodicity $m = 16$. This anomalous CP is linked to the higher growth temperature of S_{16} as compared to that of S_3 . Higher growth temperatures induce a larger interfacial width [44]. Note that Schmid *et al.* [58] showed a transition near 2.49 eV for a 1 μm Ge_7/Si_3 SL, which was attributed to the E_1 transition in the Ge-rich alloy.

Note that in this work, the studied SLs are much thinner (~ 60 nm) with a Ge content below 30%, thus excluding the possibility that the $E_{4\tau}$ emanates from Si or $\text{Si}_{1-x}\text{Ge}_x$ individual layers. Therefore, the $E_{4\tau}$ transition can only be an interface-related transition. Indeed, a further confirmation of this assessment is given by the absorption coefficients of S_3 and S_{16} , shown in panel 1(c, d), evaluated using experimental parameters (see caption of Fig. 1). This agreement between theory and experiment is further confirmed by examining the behavior of annealed SLs, as discussed below.

To enhance the interfacial broadening, SLs were subjected to rapid thermal annealing in the 780°C to 950°C temperature range under a flowing N_2 ambient gas for 50 seconds. Fig. 4(a) displays the $2\theta-\omega$ high-resolution X-ray diffraction (HRXRD) scans around the (004) diffraction order of the as-grown (blue) and annealed (red) S_3 SL. The presence of small intensity thickness fringes between the SL satellite peaks, with an angular spacing inversely proportional to the total SL thickness, is characteristic of pseudomorphic stacks with abrupt interfaces [59]. As the annealing temperature increases, the well defined SL peaks remain observable at the same angular position as for the as-grown SL. Besides, the thickness fringes become slightly less clear, which is an indication of a small interdiffusion. At the highest temperature (950°C), the SL peaks tend to become weaker and shift slightly toward the Si peak due to a larger interdiffusion. The corresponding $d^2\epsilon_2/d\omega^2$ around the $E_{4\tau}$ CP transition are exhibited in Fig. 4(b). The vertical blue and red lines represent the $E_{4\tau}$ CP peak position for the as-grown and annealed SL, respectively. Interestingly, the transition energy shift $\Delta E_{4\tau} (= E_{4\tau}^{300^\circ\text{C}} - E_{4\tau}^T)$ increases as a function of the annealing temperature from 10 meV at 780°C to 33 meV at 950°C. This redshift agrees well with the predicted theoretical results shown in Fig. 1(c). Besides, the $E_{4\tau}$ CP broadening (Γ in meV) increases with temperature from 30 meV to 50 meV which in qualitative agreement with the expected temperature effect on CP [43]. It is also worth noting that HRXRD seems to be less sensitive to interfacial broadening upon annealing at low temperature, whereas the detection of the optical fingerprint is rather straightforward hinting to the possibility to exploit the observed redshift in the $E_{4\tau}$ CP as a sensitive interface metrology. Indeed, combining the theoretical framework (Fig. 1c) and the measured shift $\Delta E_{4\tau}$ (Fig. 4b) yields a straightforward and non-destructive method to extract the interfacial broadening width in the annealed samples. A logistic regression between $\Delta E_{4\tau}$ and (4τ) was established based on the 14-band $k \cdot p$ where $\Delta E_{4\tau}$ (meV) = $73.2 / (1 + e^{-15.9((4\tau)(nm)) - 0.8})$. This demonstrates an increase in the interfacial broadening from 0.71 nm to 0.81 nm as the annealing temperature increases from 780°C to 950°C. See the Supplemental Material [15] for a detailed analysis.

In summary, atomic-level interfacial broadening was

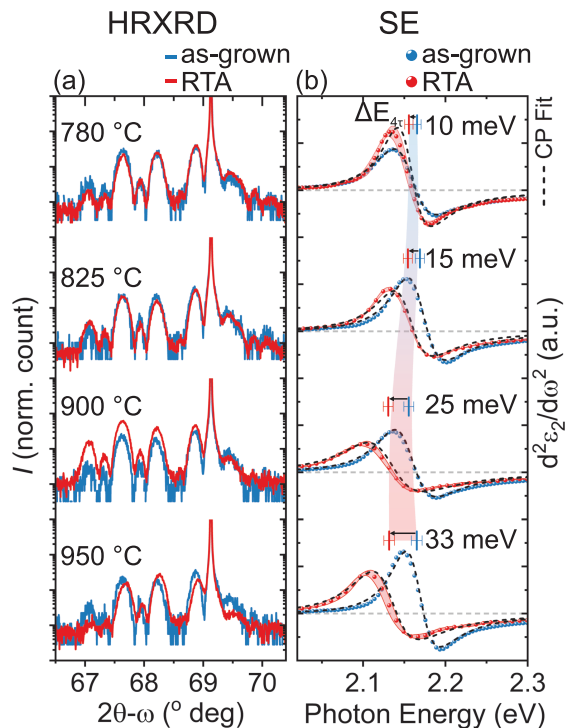


FIG. 4. **Properties of annealed SLs.** (a) XRD $\omega - 2\theta$ scans around the (004) diffraction order of the as-grown (blue) and annealed (red) S_3 SL. The annealing temperature was increased from 780°C to 950°C. (b) Second derivative statistical analysis of ε_2 is presented through the standard deviation (4σ) (red error band). The standard deviation was also used during the E_{47} CP lineshape fit (dashed lines) for both as-grown (blue) and annealed (red) S_3 samples. The interfacial broadening CP energy shift ΔE_{47} was analyzed as a function of the annealing temperature. The graded colored band (light blue to red) visualizes the redshift of the E_{47} CP as the annealing temperature increases confirming the sensitivity of this peak to interfacial broadening.

found to create localized energy states in heterostructures. This phenomenon was predicted theoretically through a rigorous theoretical formalism providing a qualitative and quantitative description of the absorption coefficient α of SLs in presence of smeared-out interfaces. The experimental measurements of CP provided a direct evidence of this behavior and identified the associated optical transitions between 2 and 2.5 eV. Furthermore, thermal annealing-induced interfacial broadening confirmed that these transitions are interface-induced. This optical fingerprint lays the foundation for a sensitive, non-destructive probe of the atomic-level broadening of interfaces.

ACKNOWLEDGEMENTS. The authors thank Mahmoud Atalla and Sebastien Koelling for fruitful discussions, Bill Baloukas for help with the spectroscopic

ellipsometry measurements, Jérôme Nicolas for help with the HRXRD measurements. O.M. acknowledges support from NSERC Canada (Discovery, SPG, and CRD Grants), Canada Research Chairs, Canada Foundation for Innovation, Mitacs, and PRIMA Québec.

AUTHORS INFORMATION. Correspondence and requests for materials should be addressed to O. Moutanabbir.

AUTHOR CONTRIBUTIONS. A.A. carried out the optical characterization. G.F. developed the 14-band $k \cdot p$ formalism. S.M. performed the APT studies. M.B. carried out the epitaxial growth of the SLs. O.M. led this research. All authors commented on the manuscript.

DATA AVAILABILITY. The data that support the findings of this study are available from the corresponding authors upon reasonable request.

* These authors contributed equally to this work.

† oussama.moutanabbir@polymtl.ca

- [1] G. Scappucci, C. Kloeffer, F. A. Zwanenburg, D. Loss, M. Myronov, J.-J. Zhang, S. De Franceschi, G. Katsaros, and M. Veldhorst, *Nature Reviews Materials* **6**, 926 (2021).
- [2] D. Paul, *Laser & Photonics Reviews* **4**, 610 (2010).
- [3] T. Grange, S. Mukherjee, G. Capellini, M. Montanari, L. Persichetti, L. Di Gaspare, S. Birner, A. Attiaoui, O. Moutanabbir, M. Virgilio, and M. De Seta, *Physical Review Applied* **13**, 044062 (2020).
- [4] T. Leontiou, J. Tersoff, and P. C. Kelires, *Physical Review Letters* **105**, 236104 (2010).
- [5] E. Luna, Á. Guzmán, A. Trampert, and G. Álvarez, *Physical Review Letters* **109**, 126101 (2012).
- [6] O. Moutanabbir, F. Ratto, S. Heun, K. Scheerschmidt, A. Locatelli, and F. Rosei, *Physical Review B* **85**, 201416 (2012).
- [7] H. Sakaki, T. Noda, K. Hirakawa, M. Tanaka, and T. Matsusue, *Applied Physics Letters* **51**, 1934 (1987).
- [8] M. Califano, N. Q. Vinh, P. J. Phillips, Z. Ikonić, R. W. Kelsall, P. Harrison, C. R. Pidgeon, B. N. Murdin, D. J. Paul, P. Townsend, J. Zhang, I. M. Ross, and A. G. Cullis, *Physical Review B* **75**, 045338 (2007).
- [9] D. Jang, D. Yakimets, G. Eneman, P. Schuddinck, M. G. Bardon, P. Raghavan, A. Spessot, D. Verkest, and A. Mocuta, *IEEE Transactions on Electron Devices* **64**, 2707 (2017).
- [10] B. P. Wuetz, M. P. Losert, S. Koelling, L. E. A. Stehouwer, A.-M. J. Zwerver, S. G. J. Philips, M. T. Mądzik, X. Xue, G. Zheng, M. Lodari, S. V. Amitonov, N. Samkharadze, A. Sammak, L. M. K. Vandersypen, R. Rahman, S. N. Coppersmith, O. Moutanabbir, M. Friesen, and G. Scappucci, ArXiv cond-mat.mes-hall **cond-mat.m**, <https://arxiv.org/abs/2112.09606> (2021).

- [11] E. L. Ivchenko, A. Y. Kaminski, and U. Rössler, *Physical Review B* **54**, 5852 (1996).
- [12] B. A. Foreman, *Physical Review Letters* **81**, 425 (1998).
- [13] F. Szmulowicz, *Physical Review B* **51**, 1613 (1995).
- [14] S. Ridene, K. Boujdaria, H. Bouchriha, and G. Fishman, *Physical Review B* **64**, 085329 (2001).
- [15] See Supplemental Material at [URL will be inserted by publisher] for details of the 14-band $k \cdot p$ theoretical formalism, as well as the SE, Raman, AFM, and APT experimental characterization, which includes Refs. [11, 12, 14, 16–43].
- [16] J. C. Tsang, P. M. Mooney, F. Dacol, and J. O. Chu, *Journal of Applied Physics* **75**, 8098 (1994).
- [17] C. G. Van de Walle, *Physical Review B* **39**, 1871 (1989).
- [18] L. D. Laude, F. H. Pollak, and M. Cardona, *Physical Review B* **3**, 2623 (1971).
- [19] B. A. Foreman, *Physical Review B* **56**, R12748 (1997).
- [20] A. B. Djurišić, T. Fritz, and K. Leo, *Journal of Optics A: Pure and Applied Optics* **2**, 458 (2000).
- [21] E. D. Palik, *Handbook of Optical Constants of Solids*, edited by E. D. Palik (Academic Press, London, 1998) p. 798.
- [22] T. B. Bahder, *Physical Review B* **41**, 11992 (1990).
- [23] J. Weber and M. I. Alonso, *Physical Review B* **40**, 5683 (1989).
- [24] H. Fujiwara, *Spectroscopic Ellipsometry: Principles and Applications* (John Wiley & Sons, Ltd, Chichester, UK, 2007) p. 388.
- [25] H. J. McSkimin, *Journal of Applied Physics* **24**, 988 (1953).
- [26] N. A. Čukarić, M. Ž. Tadić, B. Partoens, and F. M. Peeters, *Physical Review B* **88**, 205306 (2013).
- [27] I. Balslev, *Physical Review* **143**, 636 (1966).
- [28] C. G. Van de Walle and R. M. Martin, *Physical Review B* **34**, 5621 (1986).
- [29] D. J. Paul, *Journal of Applied Physics* **120**, 043103 (2016).
- [30] L. Viña, S. Logothetidis, and M. Cardona, *Physical Review B* **30**, 1979 (1984).
- [31] D. De Salvador, M. Petrovich, M. Berti, F. Romanato, E. Napolitani, A. Drigo, J. Stangl, S. Zerlauth, M. Mühlberger, F. Schäffler, G. Bauer, and P. Kelires, *Physical Review B - Condensed Matter and Materials Physics* **61**, 13005 (2000).
- [32] C. M. Herzinger, B. Johs, W. A. McGahan, J. A. Woollam, and W. Paulson, *Journal of Applied Physics* **83**, 3323 (1998).
- [33] Y. Varshni, *Physica* **34**, 149 (1967).
- [34] J. P. Dismukes, L. Ekstrom, and R. J. Paff, *The Journal of Physical Chemistry* **68**, 3021 (1964).
- [35] D. Rideau, M. Feraille, L. Ciampolini, M. Minondo, C. Tavernier, H. Jaouen, and A. Ghetti, *Physical Review B - Condensed Matter and Materials Physics* **74**, 195208 (2006).
- [36] M. El kurdi, G. Fishman, S. Sauvage, and P. Boucaud, *Physical Review B - Condensed Matter and Materials Physics* **68**, 165333 (2003).
- [37] R. R. Reeber and K. Wang, *Materials Chemistry and Physics* **46**, 259 (1996).
- [38] H. G. Tompkins, E. A. Irene, I. An, H. Arwin, C. Chen, R. W. Collins, A. S. Ferlauto, J. N. Hilfiker, J. Humlíček, J. Gerald E. Jellison, J. Lee, F. A. Modine, A. Röseler, M. Schubert, and J. A. Zapien, *Handbooks of Ellipsometry*, edited by H. G. Tompkins and E. A. Irene (William Andrew Publishing And Springer-Verlag GmbH & Co. KG, 2005) p. 1833.
- [39] M. Chandrasekhar and F. H. Pollak, *Physical Review B* **15**, 2127 (1977).
- [40] O. Madelung, U. Rössler, and M. Schulz, *Group IV Elements, IV-IV and III-V Compounds. Part b - Electronic, Transport, Optical and Other Properties*, edited by O. Madelung, U. Rössler, and M. Schulz, Landolt-Börnstein - Group III Condensed Matter, Vol. b (Springer-Verlag, Berlin/Heidelberg, 2002).
- [41] P.-F. Qiao, S. Mou, and S. L. Chuang, *Optics Express* **20**, 2319 (2012).
- [42] F. Szmulowicz, H. Haugan, and G. J. Brown, *Physical Review B* **69**, 155321 (2004).
- [43] P. Lautenschlager, M. Garriga, L. Vina, and M. Cardona, *Physical Review B* **36**, 4821 (1987).
- [44] S. Mukherjee, A. Attiaoui, M. Bauer, and O. Moutanabbir, *ACS Applied Materials & Interfaces* **12**, 1728 (2020).
- [45] D. E. Aspnes and A. A. Studna, *Physical Review B* **27**, 985 (1983).
- [46] C. M. Herzinger, B. Johs, W. A. McGahan, J. A. Woollam, and W. Paulson, *Journal of Applied Physics* **83**, 3323 (1998).
- [47] G. Raja Muthinti, M. Medikonda, T. Adam, A. Reznicek, and A. C. Diebold, *Journal of Applied Physics* **112**, 053519 (2012).
- [48] O. Dyck, D. N. Leonard, L. F. Edge, C. A. Jackson, E. J. Pritchett, P. W. Deelman, and J. D. Poplawsky, *Advanced Materials Interfaces* **4**, 1700622 (2017).
- [49] P. Snyder, B. De, K. Merkel, J. Woollam, D. Langer, C. Stutz, R. Jones, A. Rai, and K. Evans, *Superlattices and Microstructures* **4**, 97 (1988).
- [50] J. A. Woollam, P. G. Snyder, K. G. Merkel, and S. A. Alterovitz, *Materials Science and Engineering: B* **5**, 291 (1990).
- [51] J. Wagner, J. Schmitz, N. Herres, F. Fuchs, and M. Walther, *Journal of Applied Physics* **83**, 5452 (1998).
- [52] D. Aspnes, *Thin Solid Films* **89**, 249 (1982).
- [53] L. Esaki, *IEEE Journal of Quantum Electronics* **22**, 1611 (1986).
- [54] J. H. Bahng, K. J. Kim, S. H. Ihm, J. Y. Kim, and H. L. Park, *Journal of Physics: Condensed Matter* **13**, 777 (2001).
- [55] F. Ferrieu, P. Ribot, and J. L. Regolini, *Thin Solid Films* **373**, 211 (2000).
- [56] R. Lange, K. E. Junge, S. Zollner, S. S. Iyer, a. P. Powell, and K. Eberl, *Journal of Applied Physics* **80**, 4578 (1996).
- [57] C. Pickering, R. T. Carline, D. J. Robbins, W. Y. Leong, S. J. Barnett, A. D. Pitt, and A. G. Cullis, *Journal of Applied Physics* **73**, 239 (1993).
- [58] U. Schmid, J. Humlíček, F. Luke, M. Cardona, H. Presting, H. Kibbel, E. Kasper, K. Eberl, W. Wegscheider, and G. Abstreiter, *Physical Review B* **45**, 6793 (1992).
- [59] M. Py, J. P. Barnes, P. Rivallin, A. Pakfar, T. Denneulin, D. Cooper, and J. M. Hartmann, *Journal of Applied Physics* **110**, 044510 (2011).